Theoretical study of stability and electronic structure of Li(Mg,Zn)N alloys: A candidate for solid state lighting

Aron Walsh* and Su-Huai Wei
National Renewable Energy Laboratory, Golden, Colorado 80401, USA
(Received 11 September 2007; published 30 November 2007)

Using selective chemical mutation, we propose and investigate the electronic structure of an alloy with the potential to fill the green gap left open by existing InGaN based emission devices. The small mismatch between LiMgN and LiZnN, along with electronic band gaps spanning the visible range, makes them good candidates. Calculations are performed using a first-principles band structure method, with the special quasi-random structure approach employed to generate the random alloys. Comparison of LiMgN and LiZnN with their binary nitride analogs is made, and the energetic and electronic effects of alloy ordering are investigated. These alloys exhibit negative mixing enthalpies atypical of traditional binary nitride systems, which is explained in terms of the low lattice strain and the chemical bonding effects of the interstitial Li ions.

DOI: 10.1103/PhysRevB.76.195208 PACS number(s): 71.20.Nr, 73.43.Cd, 81.05.Bx

I. INTRODUCTION

Improved efficiency in the utilization of energy is urgently required to reduce our current dependence on fossil fuels. The adoption of light emitting diodes (LEDs) based on solid state materials has the capability to reduce electricity consumption for lighting applications by half.[1,2] For widespread replacement of current lighting technologies with solid state alternatives, one of the most prominent issues is the lack of efficient emission in the 500–600 nm wavelength range, which is limiting the progress of high powered white light sources. White LEDs can be produced by coating InGaN based blue emitters with a yellow phosphor; while this is acceptable in applications such as automobile headlights, the lack of a red component makes this approach unsuitable for more general use. White emitters based on a trichromatic red-green-blue (RGB) source offer better flexibility in the color rendering index which is needed for effective indoor lighting to satisfy consumers.[3] RGB white light sources are most desirable due to energy losses with the conversion of photon wavelength in phosphor containing devices.[2] The current difficulty is that there are no efficient emitters for the green part of the spectrum.

While the addition of In to GaN to form InGaN alloys can be used to fill the 500–600 nm emission range, unfortunately, this system suffers from phase separation at the desired alloy compositions, which can be understood from the strain produced by the large lattice constant mismatch of GaN (a=3.2 Å, c=5.2 Å) and InN (a=3.5 Å, c=5.7 Å). This results in very poor device efficiencies.[1] A composition of GaN and AlN (a=3.1 Å, c=5.0 Å) would help alleviate the strain, but the band gap range (3.4–6.0 eV) is too large to be considered for this application. A solution may be found through selective chemical mutation of the cations to favorably tune the band gaps, while preserving the small lattice mismatch and charge neutrality of the initial compounds. Replacing the +3 cations with an equivalent number of +2 and +1 cations can achieve such a goal. Here, we propose an alternative nitride alloy system in which Al is replaced by Li and Mg, and Ga is replaced by Li and Zn.

Filled tetrahedral semiconductors (I-II-V compounds) were first reported by Juza and Hund[4] in the 1940s and were next seen as the subject of theoretical examination in the 1980s,[5–8] resulting in the "interstitial insertion rule" which explains in detail the electronic effects of the interstitial (+1) ion on the underlying zinc-blende band structure.[5] The two materials of interest to us, LiMgN and LiZnN, have reported optical band gaps of 3.2 (Ref. 9) and 1.9 eV,[10] respectively. They have also been the focus of a number of theoretical studies investigating their electronic,[11–13] optical,[14] elastic,[15,16] and defect[17] properties. LiMgN has also received recent interest for hydrogen storage applications.[18] Alloys of these two nitrides could, in principle, bridge a 400–600 nm emission range. Most importantly, LiMgN and LiZnN have cubic lattice constants of 4.96 and 4.91 Å, ensuring that the lattice strain should not be a significant problem.

The crystal structure of LiZnN and LiMgN can be described as a cubic zinc-blende AB lattice with Li occupying half the available tetrahedral interstitial sites (Fig. 1). Viewing along the body diagonal, Mg/Zn cations sit at (0, 0, 0), with N at $(\frac{1}{4},\frac{1}{4},\frac{1}{4})$ and Li at $(\frac{1}{2},\frac{1}{2},\frac{1}{2})$. It is also feasible for Li to occupy either the $(\frac{3}{4},\frac{3}{4},\frac{3}{4})$ sites neighboring the Mg/Zn

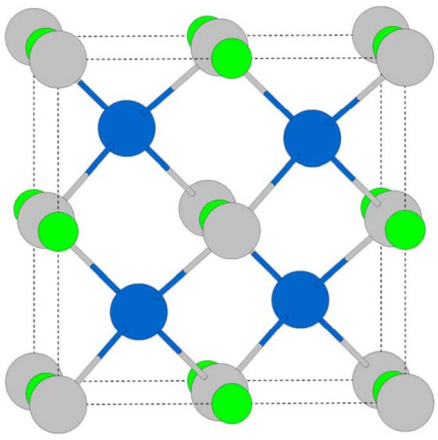

FIG. 1. (Color online) The filled tetrahedral crystal structure of LiMgN and LiZnN viewed along the (100) plane. The N atoms are colored blue (dark gray), with green (light gray) Li and gray Mg/Zn cations.

cation position (β phase) or switching with N to sit in between the Mg/Zn and N sites (γ phase).

In this study, we report the electronic structure of the $LiMg_{1-x}Zn_xN$ $(x=0,\frac{1}{4},\frac{1}{2},\frac{3}{4},1)$, alloy utilizing the special quasirandom structure (SQS) model to generate the random distribution of cations.[19] The electronic properties of the LiMgN and LiZnN ternary constituents are examined and compared to their binary analogs AlN and GaN. The natural band offsets show an increase in the energy of the valence band maxima (VBM) on transition from AlN to GaN to LiMgN to LiZnN. The band gap bowing of the random alloys is found to be almost compositionally independent at $b=0.22$ eV. The effect of alloy ordering is also investigated through examining the $x=\frac{1}{2}$ composition in four ordered superlattices. CuPt (111) alignment results in the lowest energy configuration with a band gap 80 meV lower than the random SQS structure. The uncharacteristic negative mixing enthalpies of the alloys are shown to be related to both low strain and strong structural relaxation, which is explained in relation to the effect of the Li interstitials on the frustrated chemical bonding environment between N and the +2 cations.

II. COMPUTATIONAL METHODOLOGY

The $LiMg_{1-x}Zn_xN$ alloys were modeled using a cubic supercell expansion consisting of 96 atoms. The lattice occupancies of Li and N were held constant for each system, while the SQS model[19] was applied to distribute the Mg and Zn atoms over their available lattice sites. This SQS model is constructed such that the most relevant atom-atom correlations of the 32 cations approach that of a random alloy. GaN and AlN, which favor the hexagonal wurtzite lattice, were modeled in the cubic zinc-blende structure for a more direct comparison with the compounds of interest. The total energy and band structure were obtained using density functional theory[20,21] within the generalized gradient approximation (GGA),[22] as implemented in the plane-wave code VASP.[23,24] The Zn and Ga $3d$ states were treated explicitly as valence, with the core states represented using the projector augmented wave method.[25] A plane-wave cutoff of 500 eV and a $5\times5\times5$ Monkhorst-Pack k-point grid[26] were implemented to ensure convergence to at least 1 meV/f.u. The atomic positions were fully relaxed for each system to within 1 meV/Å^3. The lattice constants of the alloys were assumed to obey Vegard's rule,[27] i.e., to be determined by a weighted average of the equilibrium ternary constituent lattice constants.

The band gap bowing coefficients were obtained from the relation

$$E_g(x) = (1-x)E_g^{\mathrm{LiMgN}} + (x)E_g^{\mathrm{LiZnN}} - bx(1-x), \qquad (1)$$

where $E_g(x)$ is the calculated band gap of the alloy at composition x. The bowing coefficient b represents the deviation of the electronic band gap of the alloy from a linear relationship of the band gaps of bulk LiMgN and LiZnN.

Our approach to calculating band alignments is similar to that of the core level x-ray photoemission spectroscopy.[28] The natural band offset between the VBM of two materials A and B can be described as

$$\Delta E_{VBM}^{A/B} = [E_{VBM}^{B} - E_{core}^{B}] - [E_{VBM}^{A} - E_{core}^{A}] + [E_{core}^{B(A/B)} - E_{core}^{A(A/B)}], \qquad (2)$$

where $E_{core}^{A}(E_{core}^{B})$ are the core energy levels for material A (B) isolated in their respective equilibrium bulk cells and $E_{core}^{A(A/B)}(E_{core}^{B(A/B)})$ are the core energy levels in a (001) oriented $A_n|B_n$ superlattice. The superlattice is calculated at a lattice constant averaged between the equilibrium lattice constants of A and B, and the convergence with respect to the number of (001) layers n is checked. The contribution arising from the VBM and core level deformation potentials have been included.[29,30] The natural offset of the conduction band is then calculated from

$$\Delta E_{CBM}^{A/B} = \Delta E_{VBM}^{A/B} + \Delta E_{g}^{A/B}, \qquad (3)$$

where $\Delta E_g^{A/B}$ is the experimental band gap difference between A and B.

III. RESULTS

A. Structural and electronic properties of LiMgN and LiZnN

The equilibrium structural and electronic parameters of LiMgN and LiZnN are listed in Table I. The optimized lattice constants of 4.999 Å for α-LiMgN and 4.933 Å for α-LiZnN are within 1% of the experimentally reported values.[9,10] Here, the larger of the two lattice constants is observed for the Mg compound, which is the reverse of the binary metal oxides,[31] indicating a decrease in ionicity from MgO to LiMgN. The α phase, with Li on the $(\frac{1}{2},\frac{1}{2},\frac{1}{2})$ lattice sites, is calculated to be significantly more stable than the β and γ phases, in agreement with the x-ray diffraction data for both LiMgN (Ref. 9) and LiZnN.[10] It is also chemically intuitive that Li, which is a +1 cation, will be most electronically satisfied when neighboring the N anion; the favorable Madelung contributions present with this configuration have previously been established for isostructural LiZnAs.[8] Due to the large energy difference of greater than 1.5 eV between the three phases for both compounds, we will only calculate the alloy properties for the α phase, i.e., assume Li occupation on $(\frac{1}{2},\frac{1}{2},\frac{1}{2})$.

The bulk moduli $[B=-(\partial p/\partial V)V]$ were obtained from an energy-volume fit to Murnaghan's equation of state.[34] Due to the GGA overestimation of the lattice constant, the calculated bulk moduli are underestimated.[35] The volume $(a_V^{\Gamma\text{-}\Gamma})$ and pressure $(a_P^{\Gamma\text{-}\Gamma})$ band gap deformation potentials were obtained from the relations

$$a_V^{\Gamma\text{-}\Gamma} = \frac{\partial E_g^{\Gamma\text{-}\Gamma}}{\partial \ln V}, \qquad (4)$$

$$a_P^{\Gamma\text{-}\Gamma} = -\left(\frac{1}{B}\right) a_V^{\Gamma\text{-}\Gamma}. \qquad (5)$$

Both LiMgN and LiZnN exhibit large negative volume deformation potentials; the corresponding pressure deformation

TABLE I. GGA calculated and experimental (in parentheses) structural and electronic properties of LiMgN and LiZnN, including the bulk moduli (B) and the band gap volume ($a_V^{\Gamma\text{-}\Gamma}$), and pressure ($a_P^{\Gamma\text{-}\Gamma}$) deformation potentials. The properties of the β and γ phases and those of zinc-blende AlN and GaN are also listed.

Material	Phase	ΔE (eV)	a^{calc} (Å)	B (Mbar)	$E_g^{\Gamma(calc)}$ (eV)	$a_V^{\Gamma\text{-}\Gamma}$ (eV)	$a_P^{\Gamma\text{-}\Gamma}$ (meV/kbar)
LiMgN	α		4.999 (4.955)	0.99	2.46 (3.20)[a]	−5.64	5.70
	β	2.08	5.067	0.77	2.40		
	γ	2.12	4.866	0.97	2.39		
LiZnN	α		4.933 (4.910)	1.12	0.59 (1.91)[b]	−4.47	4.01
	β	1.57	5.055	0.89	0.39		
	γ	2.40	4.930	0.89	0.31		
AlN			4.402 (4.360)	1.94	4.05 (6.10)[c]	−8.73	4.50
GaN			4.546 (4.500)	1.69	1.76 (3.30)[d]	−6.43	3.80

[a]Reference 9.
[b]Reference 10.
[c]Reference 32.
[d]Reference 33.

potentials are both positive, with LiMgN the larger of the two.

The electronic density of states (DOS) and band structures of both ternary nitrides are shown in Figs. 2 and 3, respectively. For LiMgN, the N $2p$ states are localized between −4 eV and 0 eV, with mixing of some Mg $3s$ states indicated at −3 eV. For LiZnN, the N $2p$ states are more dispersive, spread between −8 eV and 0 eV due to hybridization with both Zn $3d$ and Zn $4s$ at higher binding energies. In both cases, Li is fully ionized and makes no significant contributions to the occupied DOS. LiZnN exhibits a direct gap at Γ, while the indirect transition from Γ to X is almost 2 eV higher in energy. At the calculated equilibrium lattice constant, LiMgN is found to be a direct gap material, but the Γ-X splitting is only 100 meV higher than Γ-Γ. When the band structure is calculated at the experimental lattice constant, the Γ-X transition is 50 meV *lower* in energy than Γ-Γ. This effect is due to the opposite volume dependence of the band gap at the zone center in comparison with that at the X point. Compared to LiZnN, the large indirectness of the band gap is due to the fact that Mg $3d$ is unoccupied, which pushes the conduction states down at X. Similar behavior is also observed for its binary analog AlN. From the single optical study available for LiMgN, it is not evident whether the true nature of the band gap is direct or indirect.[10] The small energy difference between the Γ-Γ and Γ-X band gaps is of little consequence to this study as each of the $LiMg_{1-x}Zn_xN$ alloys exhibit a direct behavior and hence it

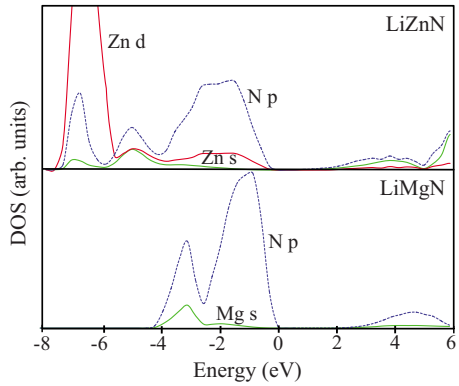

FIG. 2. (Color online) The electronic density of states of LiMgN and LiZnN. The energy zero is set to the top of the valence band.

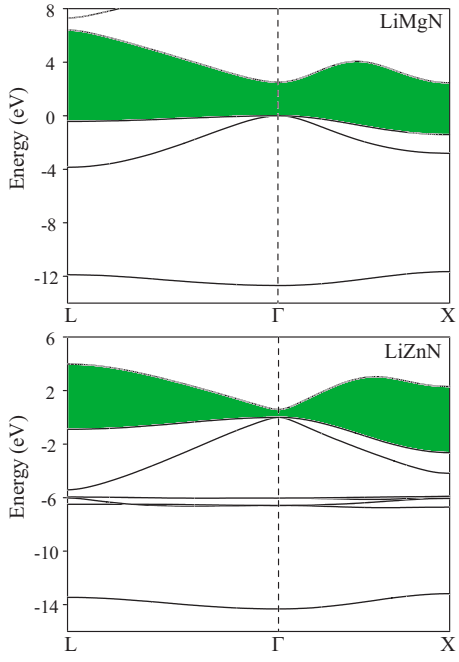

FIG. 3. (Color online) The band structures of LiMgN and LiZnN along $L\left(\frac{1}{2},\frac{1}{2},\frac{1}{2}\right)$, Γ (0, 0, 0), and $X\left(\frac{1}{2},0,\frac{1}{2}\right)$. The top of the valence band is set to 0 eV, with the area between the valence and conduction bands filled green (gray).

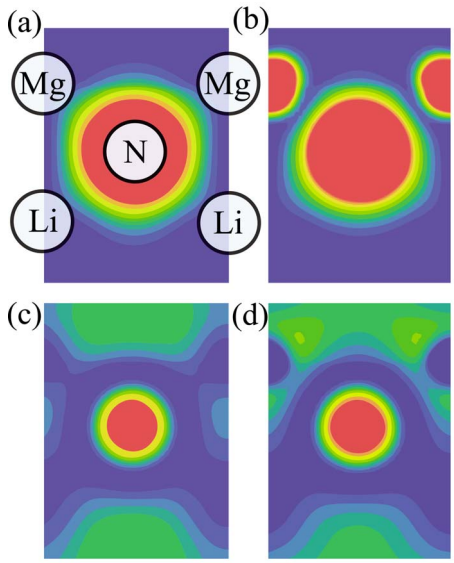

FIG. 4. (Color online) Charge density contour maps from the valence band maxima of (a) LiMgN and (b) LiZnN and the conduction band minima of (c) LiMgN and (d) LiZnN. Plots are made through the (110) plane containing N, Li, and Zn/Mg atoms. Contours are shown from 0 (blue) to 0.1 e Å^{-3} (red).

does not affect our analysis. The calculated band gaps are here reported at the experimental lattice constants.

The lowest energy gaps of 2.46 eV (LiMgN) and 0.59 eV (LiZnN) are significantly underestimated from experimental estimations, which is typical for GGA calculations. However, these systematic errors are largely canceled when calculating the bowing parameters from random alloys.[36,37] The smaller band gap of LiZnN has been attributed to the strong hybridization between the shallow Zn 3d states with N 2p resulting in an upward shift of the VBM and also the lower Zn 4s orbital energy compared to Mg 3s.[14] The same effect is observed for Mg and Zn chalcogenides.[31] This assertion is confirmed through analysis of the charge densities of the VBM and conduction band minimum (CBM) states. Figure 4 contains contour plots for a slice through the (110) plane, containing Li, N, and Mg/Zn sites. For LiMgN, both the VBM and CBM are mainly localized on the nitrogen. For LiZnN, p-d coupling results in additional Zn 3d based contributions to the VBM. The CBM of LiZnN is again dominated by N but with more contributions from the Zn sites.

B. Comparison with AlN and GaN

The properties of GaN and AlN are also listed in Table I. The calculated direct band gaps of 4.05 eV (AlN) and 1.76 eV (GaN) are in the region of 1 eV greater than their corresponding ternary nitrides. The values of $a_V^{\Gamma\text{-}\Gamma}$ for AlN (−8.73 eV) and GaN (−6.52 eV) are more negative than those calculated for LiMgN and LiZnN, in line with a decrease in the covalency of the ternary nitrides.[38] However, as the calculated bulk moduli of 0.99 Mbar for LiMgN and 1.12 Mbar for LiZnN are almost half the values of GaN and AlN, the resulting pressure deformation potentials for the

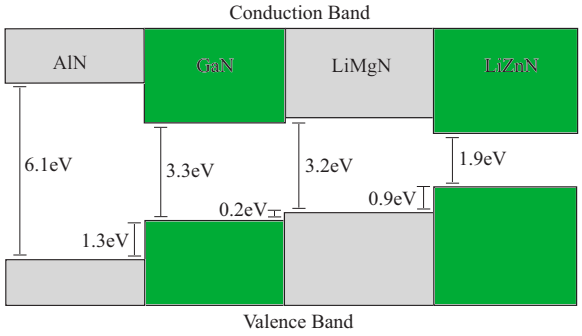

FIG. 5. (Color online) The GGA natural band offset between cubic AlN, LiMgN, GaN, and LiZnN.

ternary nitrides are greater. The smaller bulk moduli of LiMgN and LiZnN are related to the lattice expansion induced by the presence of the interstitial Li ions and the increased ionicity.

The natural band offsets, as shown in Fig. 5, were calculated according to Eq. (2). The shallow Ga and Zn 3d states increase the energy of the VBM for GaN and LiZnN compared to AlN and LiMgN. The lower CBM (and contributions to the higher VBM) of the ternary nitrides compared to their binary analogs is due to the larger volume of the ternary compounds caused by the Li interstitials; for example, the direct band gap of LiMgN calculated at the lattice constant of AlN is increased from 2.46 to 5.57 eV. For GaN/LiZnN, the observed differences are also related to the higher binding energy of the occupied Ga 3d states relative to Zn, decreasing the strength of p-d coupling. Across the series, the relative energies of the VBM increase by 1.3 eV from AlN to GaN, 0.2 eV from GaN to LiMgN, and a further 0.9 eV from LiMgN to LiZnN. Following the guidelines set by the phenomenological doping limit rules,[39–42] the higher VBM and lower CBM of the ternary nitrides should result in improved p- and n-type dopability over AlN and GaN.

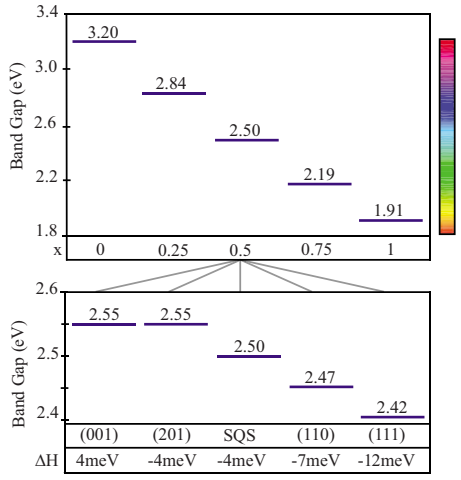

FIG. 6. (Color online) Predicted band gaps, using the averaged calculated bowing coefficient of 0.22 eV, along the compositional range of the $LiMg_{1-x}Zn_xN$ random alloy (upper) and for the ordered $LiMg_{0.5}Zn_{0.5}N$ superlattices (lower). The corresponding visible color spectrum is drawn in the right panel.

TABLE II. Calculated band gaps (E_g), bowing coefficients (b), and mixing enthalpies (ΔH) at each alloy composition. The predicted values of E_g are obtained by applying the averaged bowing coefficient (0.22 eV) to the experimental band gaps of LiMgN and LiZnN.

Material	Calculated E_g (eV)	b (eV)	Predicted E_g (eV)	ΔH (meV)
LiMgN	2.46		3.20	
$LiMg_{0.75}Zn_{0.25}N$	1.95	0.23	2.84	−3.6
$LiMg_{0.5}Zn_{0.5}N$	1.47	0.22	2.50	−4.3
$LiMg_{0.25}Zn_{0.75}N$	1.02	0.20	2.19	−4.0
LiZnN	0.59		1.91	

C. Properties of the random alloys

The calculated band gaps (E_g), bowing coefficients (b), and mixing enthalpies (ΔH) for each of the random $LiMg_{1-x}Zn_xN$ alloys are listed in Table II. The mixing enthalpies were calculated from the relation

$$\Delta H(x) = E_x - [(1-x)E_{\mathrm{LiMgN}} + xE_{\mathrm{LiZnN}}], \tag{6}$$

where E_x is the total energy of the alloy at composition x and $E_{\mathrm{LiMgN}}/E_{\mathrm{LiZnN}}$ are the total energies of the bulk ternary nitrides. These were calculated using an equivalent k-point mesh and basis set to ensure the best possible numerical precision. It is typical for bulk nitride alloys to exhibit positive mixing enthalpies relative to their constituents, with negative energies only accessible under conditions of epitaxial constraint.[43] However, for this system, negative mixing enthalpies in the region of −4 meV/f.u. are calculated for each composition, likely arising from the absence of lattice strain and the presence of attractive chemical interactions. The origin of this stability will be discussed in more detail in Sec. III D.

The band gap bowing coefficients were derived by substituting the calculated electronic band gaps into Eq. (1). The bowing is found to be very low and almost compositionally independent (0.21–0.23 eV), indicative of a well behaved alloy. The averaged value of 0.22 eV implies deviations of only 41 meV $\left(x=\frac{1}{4},\frac{3}{4}\right)$ and 55 meV $\left(x=\frac{1}{2}\right)$ from a linear interpolation of LiMgN and LiZnN. Through applying this averaged bowing coefficient to the experimental band gaps of the ternary Mg and Zn nitrides, we can make a more precise prediction of the observable band gap at each composition. These results are listed in Table II and are also graphed in Fig. 6. As illustrated in the graph, the predicted band gaps of the alloys smoothly chart the majority of the visible wavelength spectrum on transition from LiZnN (1.91 eV, 653 nm) to LiMgN (3.20 eV, 388 nm).

TABLE III. A comparison of the energetic and electronic properties of the random and ordered configurations of $LiMg_{0.5}Zn_{0.5}N$. ΔH is the mixing enthalpy relative to LiMgN and LiZnN.

$LiMg_{0.5}Zn_{0.5}N$	ΔH (meV)	Calculated E_g (eV)	Predicted E_g (eV)
SQS structure	−4.3	1.47	2.50
(001) (1×1)	4.1	1.52	2.55
(110) (2×2)	−7.2	1.44	2.47
(111) (1×1)	−11.7	1.39	2.42
(201) (2×2)	−4.0	1.52	2.55

D. Effect of alloy ordering

In the preceding section, we have assumed a random distribution of Mg and Zn ions over their available lattice sites. Depending on the preparatory conditions, this may not be the case, especially when the formation energy is negative; spontaneous superlattice ordering has been predicted and observed in a wide range of semiconductor systems and can have an important influence on the physical properties of the alloy.[43–49] The nature of the cation distribution represents a balance between both steric and electronic induced contributions. To investigate the effect of Mg and Zn ordering in this system, in addition to the random SQS generated configuration, we have also calculated the stoichiometric $LiMg_{0.5}Zn_{0.5}N$ composition in four ordered superlattice configurations: alternating planes of Mg and Zn aligned along (i) (001) in a (1×1) $P\bar{4}m2$ superlattice (CuAu type), (ii) (110) in a (2×2) $Pmn21$ superlattice (Y2 type), (iii) (111) in a (1×1) $R3m$ superlattice (CuPt type), and (iv) (201) in a (2×2) $I\bar{4}2d$ superlattice (chalcopyrite type). These orderings are illustrated in Fig. 7 and the resulting energetic and electronic data are listed in Table III.

The mixing enthalpies of each configuration all lay within a small 16 meV energy range. The energetic ordering of

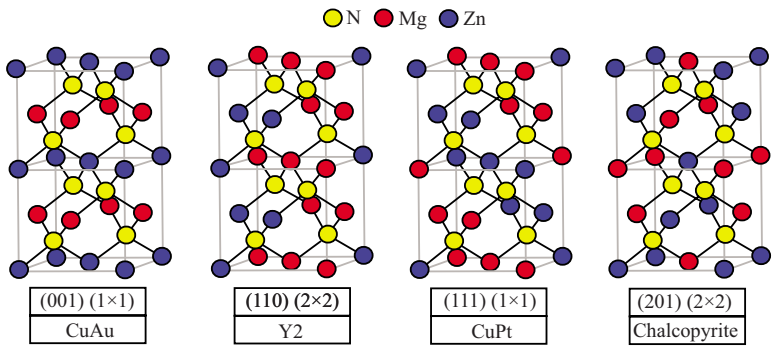

FIG. 7. (Color online) Schematic representation of the four ordered cation $LiMg_{0.5}Zn_{0.5}N$ structures considered. Li has been removed for clarity of the remaining atoms.

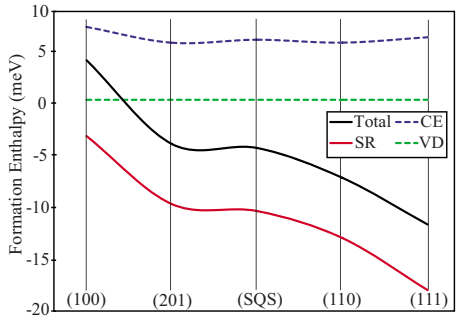

FIG. 8. (Color online) Breakdown of the mixing enthalpies of the four ordered and single random (SQS) $LiMg_{0.5}Zn_{0.5}N$ alloys into volume deformation (VD), charge exchange (CE), and structural relaxation (SR) terms.

$\Delta H^{001}_{\mathrm{CuAu}} > \Delta H^{201}_{chalcopyrite} > \Delta H^{random}_{SQS} > \Delta H^{110}_{Y2} > \Delta H^{111}_{\mathrm{CuPt}}$ is consistent with previous observations[43,45] that while (111) CuPt alignment results in the highest energy configuration for systems with large lattice constant mismatch, in low mismatch systems, it is among the most favorable; the inverse holds true for (201) chalcopyrite ordering. To gain a better understanding of the origin of the relative lattice stabilities, we have expanded the mixing enthalpies into three elemental components:

$$\Delta H(x) = \Delta E_{VD} + \Delta E_{CE} + \Delta E_{SR}. \quad (7)$$

(i) Volume deformation (E_{VD}): the energetic cost of the volume change associated with compressing (expanding) the ternary nitrides to volume V on forming the $x=\frac{1}{2}$ alloy. This term is independent of the specific type of ordering.

(ii) Charge exchange (E_{CE}): contains contributions from the chemical differences between the two cations and is calculated from the total energy of the unrelaxed superlattices at volume V.

(iii) Structural relaxation (E_{SR}): the energy gain due to the full relaxation of the internal coordinates at volume V within the given space group symmetry.

For nearly lattice matched binary alloys, the volume deformation and structural relaxation terms would be expected to be small. Indeed, for this system, the small mismatch and low bulk moduli result in almost negligible contributions from E_{VD}, as shown in Fig. 8. Surprisingly, the positive charge exchange contributions are more than compensated by the strong structural relaxations, resulting in the overall negative mixing enthalpies. The charge exchange is positive due to the destabilizing effect of the reduced Madelung interaction caused by charge averaging of the two alloyed cations.[43] While E_{CE} is on the order of +6 meV, E_{SR} results in stabilization ranging from +3 meV for the CuAu superlattice to +18 meV for CuPt ordering. The enhanced stabilization of (110) Y2 and (111) CuPt ordering is due to the fact that these structures have two nitrogen coordination environments of 3Mg-N-Zn and Mg-N-3Zn, which gain more Coulomb energy than the 2Mg-N-2Zn environments present in the (001) CuAu and (201) chalcopyrite structures (Fig. 7).

We find that the favorable E_{SR} term results from substantial relaxation of the N-Li, N-Mg, and N-Zn bonding environments, as seen in Table IV. The most striking change upon relaxation is the large variation in the N-Li bond lengths and the inversion of the N-Mg and N-Zn interatomic distances. In the bulk ternary nitrides, distances of 2.14 and 2.16 Å are found for N-Zn and N-Mg, respectively, which have the same order as the more covalent Mg and Zn binary chalcogenides,[31] while in the relaxed alloys, the magnitudes are reversed, i.e., the same order as the more ionic MgO and ZnO.[31] This is because in the ternary compounds with high symmetry, the ideal oxidation states and bond lengths are not reached, i.e., unlike in the binary analog compounds, the ternary nitrides are intrinsically strained. Formation of the quaternary nitride alloy reduces the symmetry and allows the system to relax more closely to their ideal oxidation states and bond lengths. As such, the contraction of the N-Mg interatomic distances upon forming the alloys can be understood in terms of increased ionic character, which is gained through more charge transfer to the neighboring Li ions. Decreased cation size with increased ionicity is commonly observed.[50–52] For the (110) Y2 and (111) CuPt ordered structures, the nitrogen coordinated to three Mg ions results in substantially expanded N-Li distances relative to those around the nitrogen coordinated to three Zn, with the greatest difference of 0.07 Å present for the (111) superlattice. This concerted structural relaxation is less in the higher symmetry (001) CuAu and (201) chalcopyrite superlattices with only 2Mg-N-2Zn coordination environments.

TABLE IV. The averaged anion-cation interatomic distances in the relaxed ordered $LiMg_{0.5}Zn_{0.5}N$ alloys.

Ordering	N-Mg (Å)	N-Zn (Å)	N-Li (Å)
(001) (CuAu)	2.14	2.16	2.15
(110) (Y2)	3×2.14	1×2.14	2.17
	1×2.15	3×2.16	2.12
(111) (CuPt)	3×2.14	1×2.13	2.18
	1×2.15	3×2.16	2.11
(201) (chalcopyrite)	2.14	2.16	2.15

Preliminary calculations on $LiMg_{1-x}Zn_xP$ indicates that this system does not follow the same trend as the quaternary nitride alloys, with smaller relaxation contributions and positive mixing enthalpies across the compositional range.[53] This is because phosphides have smaller strain (elastic) energy than the nitrides and are more covalent, so there is no size inversion between Mg and Zn due to reduced ionicity.

The calculated electronic band gaps of the random SQS, (100), and (201) configurations are close in energy, in the region of 2.5 eV, while the more stable (111) and (110) ordered configurations result in reduced band gaps of 2.42 and 2.47 eV, respectively. (111) CuPt alignment is known to result in the largest band level repulsions between the Γ and L states, causing the CBM states to shift down in energy, resulting in its lower fundamental gap.[48] As we are only considering fully ordered systems in our simulations, these ordering effects will be exaggerated compared to the true equilibrium mixture. The results do at least infer that there will be some opportunity to fine tune the band gap through

altering temperature and growth conditions with an 80 meV spread between the random alloy and the stable CuPt superlattice.

IV. CONCLUSION

We have reported the results of an electronic structure study of the ternary nitrides LiMgN and LiZnN, as well as their quaternary alloys, using the SQS approach to generate the random structures. The calculated equilibrium lattice vectors confirm the low lattice mismatch between LiMgN and LiZnN. Band alignment between LiMgN, LiZnN, AlN, and GaN illustrate that the lower band gap of LiZnN arises from a higher energy VBM relative to LiMgN, a consequence of *p-d* coupling. The ternary nitrides exhibit higher VBM and lower CBM levels relative to AlN and GaN, suggesting that LiMgN and LiZnN should be more readily doped. Low and almost compositionally independent band gap bowing of 0.22 eV is calculated, indicative of a well behaved alloy. However, the calculated negative mixing enthalpies are not typical of other binary nitride semiconductor alloys, which result from the increased structural freedom in the low symmetry quaternary nitride environment. Examination of ordering for the $LiMg_{0.5}Zn_{0.5}N$ composition showed that the (111) CuPt and (110) Y2 ordered superlattices can offer enhanced stability over a random distribution of cations. These stable ordered structures result in electronic band gaps of up to 80 meV lower than the random alloy. We have therefore demonstrated the potential of an alloy system that has a band gap tunable throughout the visible range, with small mismatch and low bowing. Experimental tests for our predictions are called for.

ACKNOWLEDGMENTS

We would like to thank Sarah Kurtz for useful discussions. This work was supported by the U.S. Department of Energy under Contract No. DE-AC36-99GO10337.

*aron_walsh@nrel.gov

[1] DOE, *Energy Savings Potential of Solid-State Lighting in General Illumination Applications* (Navigant Consulting, Washington, DC, 2006).
[2] E. F. Schubert, J. K. Kim, H. Luo, and J. Q. Xi, Rep. Prog. Phys. **69**, 3069 (2006).
[3] DOE, *Basic Research Needs for Solid-State Lighting* (Basic Energy Sciences, Washington, DC, 2006).
[4] R. Juza and F. Hund, Naturwiss. **33**, 121 (1946).
[5] A. E. Carlsson, A. Zunger, and D. M. Wood, Phys. Rev. B **32**, 1386 (1985).
[6] D. M. Wood, A. Zunger, and R. de Groot, Phys. Rev. B **31**, 2570 (1985).
[7] H. W. A. M. Rompa, M. F. H. Schuurmans, and F. Williams, Phys. Rev. Lett. **52**, 675 (1984).
[8] S.-H. Wei and A. Zunger, Phys. Rev. Lett. **56**, 528 (1986).
[9] K. Kuriyama, K. Nagasawa, and K. Kushida, J. Cryst. Growth **237-239**, 2019 (2002).
[10] K. Kuriyama, T. Kato, and T. Tanaka, Phys. Rev. B **49**, 4511 (1994).
[11] H. P. Li, Z. F. Hou, M. C. Huang, and Z. Z. Zhu, Chin. Phys. Lett. **20**, 114 (2003).
[12] L. H. Yu, K. L. Yao, and Z. L. Liu, Physica B **353**, 278 (2004).
[13] H. C. Kandpal, C. Felser, and R. Seshadri, J. Phys. D **39**, 776 (2006).
[14] F. Kalarasse and B. Bennecer, J. Phys. Chem. Solids **67**, 1850 (2006).
[15] A. Bouhemadou, R. Khenata, and F. Zerarga, Solid State Commun. **141**, 288 (2007).
[16] F. Kalarasse and B. Bennecer, J. Phys. Chem. Solids **67**, 846 (2006).
[17] K. Toyoura, F. Oba, T. Ninomiya, A. Kuwabara, and I. Tanaka, J. Phys.: Condens. Matter **19**, 046201 (2007).
[18] J. Lu, Z. Z. Fang, Y. J. Choi, and H. Y. Sohn, J. Micro/Nanolith. MEMS MOEMS **111**, 12129 (2007).
[19] S.-H. Wei, L. G. Ferreira, J. E. Bernard, and A. Zunger, Phys. Rev. B **42**, 9622 (1990).
[20] P. Hohenberg and W. Kohn, Phys. Rev. **136**, B864 (1964).
[21] W. Kohn and L. J. Sham, Phys. Rev. **140**, A1133 (1965).
[22] J. P. Perdew, K. Burke, and M. Ernzerhof, Phys. Rev. Lett. **77**, 3865 (1996).
[23] G. Kresse and J. Furthmüller, Phys. Rev. B **54**, 11169 (1996).
[24] G. Kresse and J. Furthmüller, Comput. Mater. Sci. **6**, 15 (1996).
[25] P. E. Blöchl, Phys. Rev. B **50**, 17953 (1994).
[26] H. J. Monkhorst and J. D. Pack, Phys. Rev. B **13**, 5188 (1976).
[27] L. Vegard, Z. Phys. **5**, 17 (1921).
[28] S. P. Kowalczyk, J. T. Cheung, E. A. Kraut, and R. W. Grant, Phys. Rev. Lett. **56**, 1605 (1986).
[29] Y. H. Li, X. G. Gong, and S.-H. Wei, Phys. Rev. B **73**, 245206 (2006).
[30] Y. H. Li, X. G. Gong, and S.-H. Wei, Appl. Phys. Lett. **88**, 042104 (2006).
[31] D. Segev and S.-H. Wei, Phys. Rev. B **68**, 165336 (2003).
[32] J. Li, K. B. Nam, M. L. Nakarmi, J. Y. Lin, H. X. Jiang, P. Carrier, and S.-H. Wei, Appl. Phys. Lett. **83**, 5163 (2003).
[33] G. Ramírez-Flores, H. Navarro-Contreras, A. Lastras-Martínez, R. C. Powell, and J. E. Greene, Phys. Rev. B **50**, 8433 (1994).
[34] F. D. Murnaghan, Proc. Natl. Acad. Sci. U.S.A. **30**, 244 (1944).
[35] A. Janotti, S.-H. Wei, and D. J. Singh, Phys. Rev. B **64**, 174107 (2001).
[36] C. Y. Moon, S.-H. Wei, Y. Z. Zhu, and G. D. Chen, Phys. Rev. B **74**, 233202 (2006).
[37] S.-H. Wei and A. Zunger, Phys. Rev. Lett. **76**, 664 (1996).
[38] S.-H. Wei and A. Zunger, Phys. Rev. B **60**, 5404 (1999).
[39] S. B. Zhang, S.-H. Wei, and A. Zunger, Phys. Rev. Lett. **84**, 1232 (2000).
[40] S. B. Zhang, S.-H. Wei, and A. Zunger, J. Appl. Phys. **83**, 3192 (1998).
[41] S. B. Zhang, S.-H. Wei, and A. Zunger, Phys. Rev. B **63**, 075205 (2001).
[42] S.-H. Wei, Comput. Mater. Sci. **30**, 337 (2004).
[43] J. E. Bernard, L. G. Ferreira, S.-H. Wei, and A. Zunger, Phys.

Rev. B **38**, 6338 (1988).
[44] G. P. Srivastava, J. L. Martins, and A. Zunger, Phys. Rev. B **31**, 2561 (1985).
[45] J. E. Bernard, R. G. Dandrea, L. G. Ferreira, S. Froyen, S.-H. Wei, and A. Zunger, Appl. Phys. Lett. **56**, 731 (1990).
[46] C. Y. Moon, J. Li, S.-H. Wei, Adele Tzu-Lin Lim, and Y. P. Feng, Phys. Rev. B **74**, 205203 (2006).
[47] J. Ni, X. C. Lai, and B. L. Gu, J. Appl. Phys. **73**, 4260 (1993).
[48] S.-H. Wei and A. Zunger, Phys. Rev. B **39**, 3279 (1989).
[49] N. E. Christensen, S.-H. Wei, and A. Zunger, Phys. Rev. B **40**, 1642 (1989).
[50] D. J. Payne, R. G. Egdell, D. S. L. Law, P. A. Glans, T. Learmonth, K. E. Smith, J. H. Guo, A. Walsh, and G. W. Watson, J. Mater. Chem. **17**, 267 (2007).
[51] R. Shannon, Acta Crystallogr., Sect. A: Cryst. Phys., Diffr., Theor. Gen. Crystallogr. **32**, 751 (1976).
[52] A. Walsh, S.-H. Wei, Y. Yan, M. M. Al-Jassim, J. A. Turner, M. Woodhouse, and B. A. Parkinson, Phys. Rev. B **76**, 165119 (2007).
[53] A. Walsh and S.-H. Wei (unpublished).